Investigating reliability problems of high tin content solder alloys (Final report)

The results of the five-year research project about high Sn content solder alloy can be ordered around the following four main topics: (i) tin pest phenomenon in high Sn content alloys; (ii) reliability of high Sn content thin film layers; (iii) quality and application of composite solder alloys; and (vi) reliability of composite solder alloys. In the next part of the research report, the main findings will be presented for each topic.

1. Tin pest phenomenon in high Sn content alloys

The allotropic transition of the metallic β-Sn to non-metallic α-Sn was investigated in Sn99Cu1 and Sn99Ag0.3Cu0.7 solder alloys [1]. Bulk solder bars were prepared and inoculated with InSb, CdTe, and α -Sn. Samples were stored at -18 °C for 10 weeks. The allotropic transition was characterized by electrical resistance measurements. The transition showed characteristic differences in the different alloys and inoculators, like different nucleation, growth, and saturation stages. Generally, the Sn99Cu1 alloy showed more susceptibility against α-Sn transition than the Sn99Ag0.3Cu0.7 alloy, which performed the transition only in the case of α-Sn inoculation. This might be explained by the presence of Ag in the alloy since Ag_3Sn IMCs in the solder bulk can decrease grain-boundary diffusion [2, 3].

Although the presence of α-Sn initiates the transition faster than the other inoculators, but the non-tin inoculators result in much more serious destruction of the samples. InSb inoculator initiated the tin pest phenomenon with a shorter nucleation time than CdTe, but finally, very high electrical resistance increase, and decomposition of the samples occurred in the case of both inoculators. In the case of InSb inoculator, the transition reached the saturation phase, while with CdTe, it did not. The intense vertical expansion of the transition in the case of InSb and CdTe inoculators was probably caused by their diffusion in the sample body [1-3].

The effect of recrystallization of 99.3Sn0.7Cu solder alloy on the allotropic transition of β to α-Sn has also been investigated [4]. Half of the samples were used as the reference, and the other half were annealed at 180 °C for 72 hours, which caused the recrystallization of the alloy. Then the samples were stored at -10 °C and -20 °C. The resistance increase of all samples could be expressed with the same exponential equation but with different exponents (Fig. 1). The transient nucleation time was 2 and 10 times shorter, and the exponent of the resistance increase was 2.5 and 10 times higher at -20 °C than at -10 °C test. The recrystallization suppressed the tin pest phenomenon considerably.

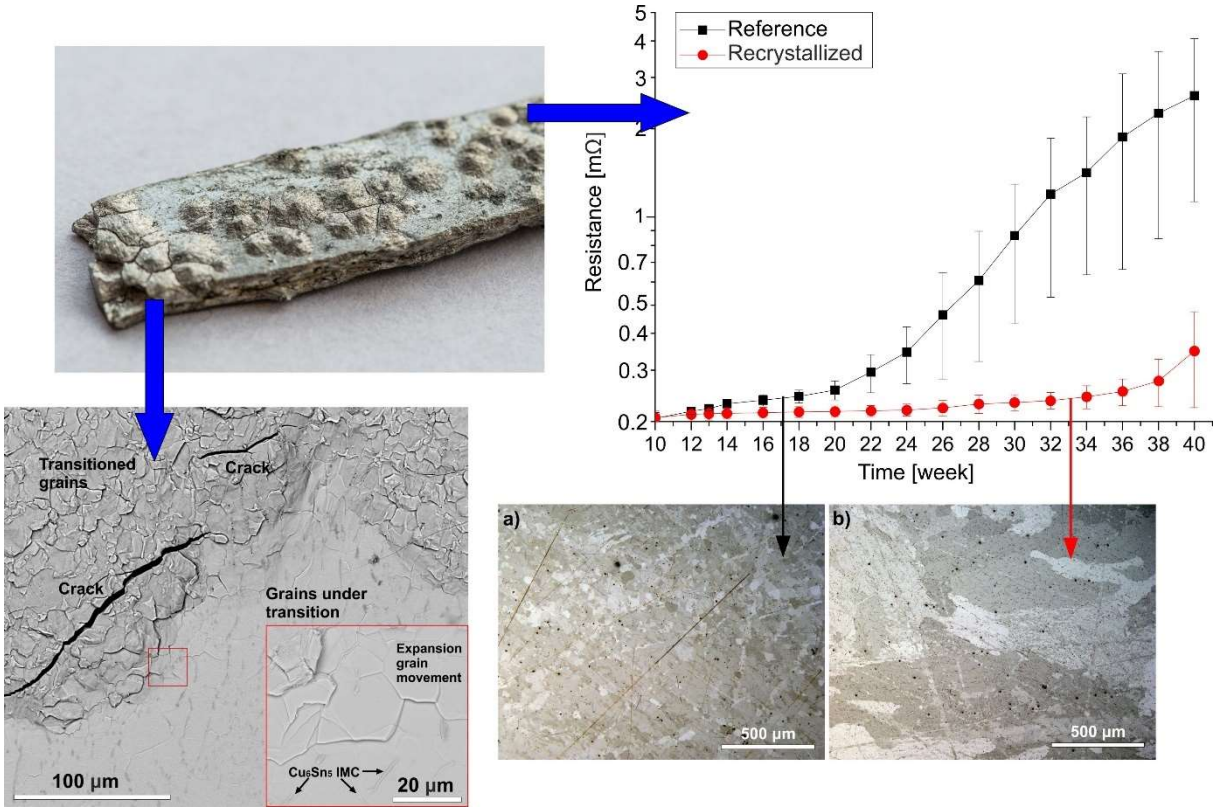

Fig. 1. The tin pest phenomenon: a sample during the transition (left upper and lower corner), resistance increase (right upper corner), and the effect of recrystallization on the Sn grain size (right lower corner) [4].

The exponents of the resistance changes in the case of recrystallized samples were only 64 % (-10 ºC) and 17 % (-20 ºC) of the exponents in the case of the reference samples (Fig. 1). The positive effect of recrystallization can be explained by the grain boundary decrease (grain size increase, as visible in Fig. 1 right lower corner) and by the decrease of vacancies and dislocations where the heterogeneous nucleation could occur [4].

2. Reliability of high Sn content thin film layers

One base of a proper solder joint is the proper solder pad, which means Cu wiring with a 0.4 - 2µm thick surface finishing, usually made from pure or high Sn content alloys. It is already known that the Sn film layers on Cu substrate have high Sn whisker growth susceptibility. However, neither the whisker growth characteristics nor the Cu substrate properties' role were known before. At the beginning, we investigated two different factors of the layer structure: the Sn layer thickness and the surface roughness of the Cu substrate. Samples were prepared by vacuum evaporation from 99.99Sn with 0.4, 1, and 2µm layer thickness on polished and unpolished Cu substrates.

The first aim was to obtain more information about the whiskering behaviour of Sn films in the early stage of the life cycle [5]. For this study, the samples with 2μm Sn layer on polished and unpolished Cu substrates were used. Samples were stored at room temperature for 10 weeks. Whisker development was observed by SEM. It was found that the large compressive stress in the Sn layer due to the intermetallic (IMC) formation initiates the whisker development. It was started after 1 day, and most of the whiskers formed up to 10 days after the Sn deposition. Later, only the length of the whiskers increased until the end of the study. The number of the developed whiskers was not extremely high, but their length was significant since almost only filament-type whiskers were developed. The whisker density reached 40 and 75pcs./mm2 on the unpolished and polished Cu substrates, respectively. The longest detected Sn whisker was 420μm and 200μm on the samples with unpolished and polished Cu substrates, respectively. Generally, the samples with rough Cu surfaces produced fewer but longer whiskers than the samples with polished Cu surfaces [5].

Further investigations of the relationship between the Cu substrate roughness and the whisker growth were done [6]. Pure Sn was vacuum-evaporated onto unpolished and mechanically polished Cu substrates with 1μm and 2μm layer thicknesses. The samples were stored in room conditions for 60 days. The considerable stress of rapid intermetallic layer (IMC) formation resulted in intensive whisker formation, even in some days after the layer deposition (Fig. 2). Sn thin-film on unpolished Cu substrate produced less but longer whisker than that on polished Cu substrate, which could be explained by the differences in the IMC formation.

Unpolished Cu substrate produced a non-uniform IMC layer with wedge-shaped IMC grains, which resulted in rarer but long whiskers at stress peaks of the IMC wedges. Polished Cu substrate produced a uniform IMC layer with evenly high stress levels on the Sn layer, which produced a lot but short filament-type whiskers. The decrease of the layer thickness increased considerably the number of tin whiskers and moderately the length of them. The amount increase was due to the development of nodule-type whiskers on the thinner Sn thin-film due to the easier diffusion of Cu atoms into the whiskers, which can yield the formation of nodule-type whiskers [6].

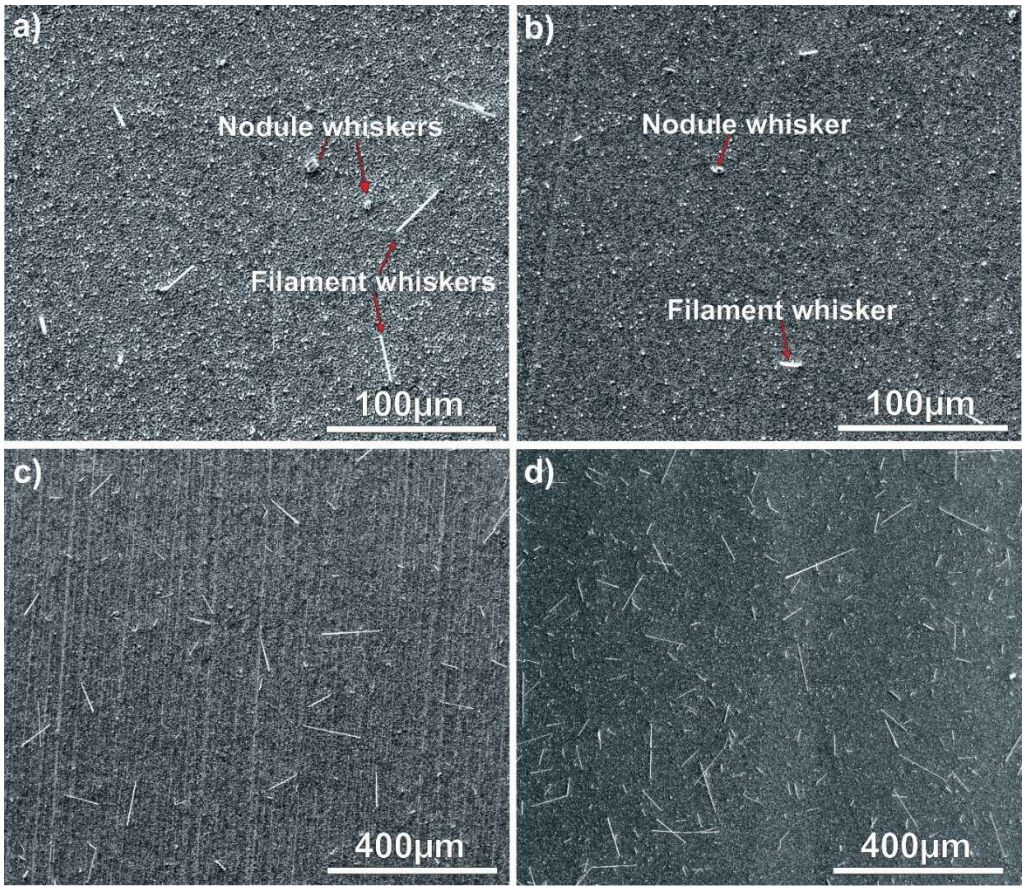

Fig. 2. Whiskers on the samples: a) filament- and nodule-type whiskers on sample S2 after 7 days; b) filament- and nodule-type whiskers on sample S3 after 7 days; c) numerous 50–100 µm long filament whiskers on sample S2 after 60 days; d) numerous filament (50–200µm long) and nodule-type whiskers on sample S3 after 60 days [6].

The investigations were continued with the kinetics of Sn whisker growth [7]. Sn film layers were deposited on a Cu substrate with 0.5 and 1 µm thicknesses. The samples were stored in room conditions (22 ± 1 °C/50 ± 5RH%) for 60 days [7]. It was found that the fast Cu_6Sn_5 intermetallic (IMC) formation resulted in considerable mechanical stress in the Sn layer, which initiated intensive whisker growth right after the layer deposition. The maximum detected growth rate reached 2.15 µm/h between the 5^{th} and 7^{th} day of the experiments. In this period, even the average growth rate was over 0.75 µm/h. 10 days after the Sn layer deposition, the growth rates started to decrease, and in the second half of the study, only very low values were detected.

The observed kinetics of the whisker growth was determined by the cross-correlation of the stress relaxation ability of the Sn layer and the amount of Sn atoms for whisker growth. The thinner Sn layer started whisker growth right after the layer deposition, but available Sn atoms

were consumed quickly by the IMC formation. The thicker Sn layer relaxed the mechanical stress longer, but it could maintain the whisker growth longer. Generally, the decrease of the Sn film-layer thickness increased the number of whiskers but did not increase the maximal length of the whisker considerably. The high filament whisker growth rates could be caused by the interface flow mechanism, which could be initiated by the IMC layer growth itself. A correlation was found between the types of the whiskers and the morphology of the IMC layer underneath them (Fig. 3.).

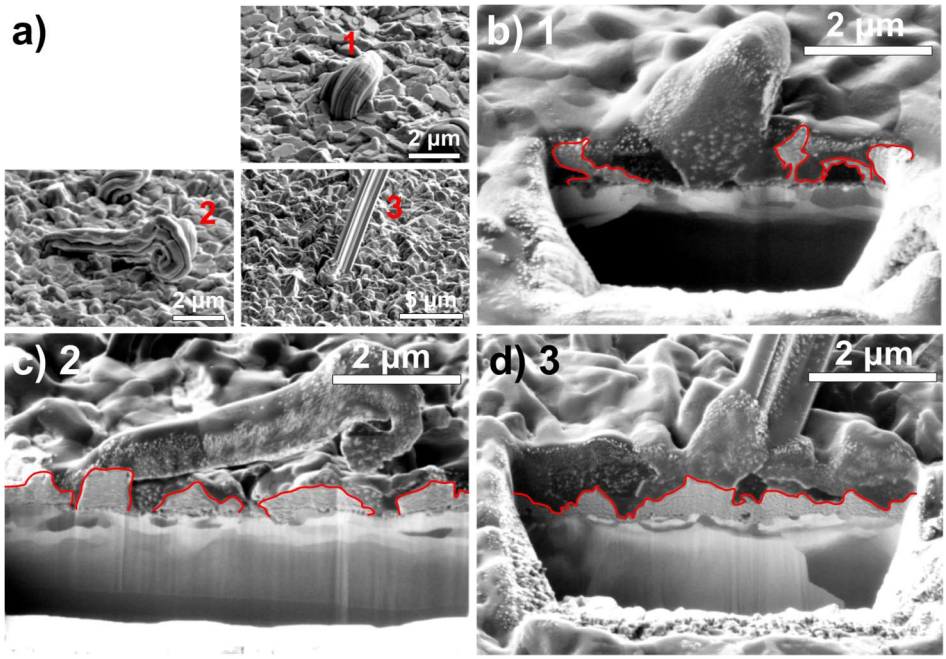

Fig. 3. FIB examinations of the layer structure under the different type of Sn whiskers after 60 days: a) the investigated whiskers; b) hillock-type whisker on 1 µm thick Sn layer; c) nodule-type whisker on 0.5 µm thick Sn layer; d) filament-type whisker on 1 µm thick Sn layer [7].

Under the hillock-type whiskers, the IMC layer was usually uneven with scallop-type IMC grains. Under the nodule-type and filament-type whiskers, the IMC layer was usually more continuous layer-like [7].

Our further aim was to study the relationship between the crystallographic structure of Cu-Sn IMC grains and Sn whisker growth [8]. For this study, samples with 0.4µm Sn layer on unpolished Cu substrates were used. The samples were stored at room temperature for 1 month. Different types of whiskers (nodule and filament) and the layer structure underneath were studied with a Scanning Ion Microscope (SIM) and Transmission Electron Microscopy (TEM). The TEM investigation showed that not only the thickness of the IMC layer and the shape of the Cu_6Sn_5 grains (Fig. 4.b) affect Sn whisker development, but also the crystallographic structure of the IMC grains.

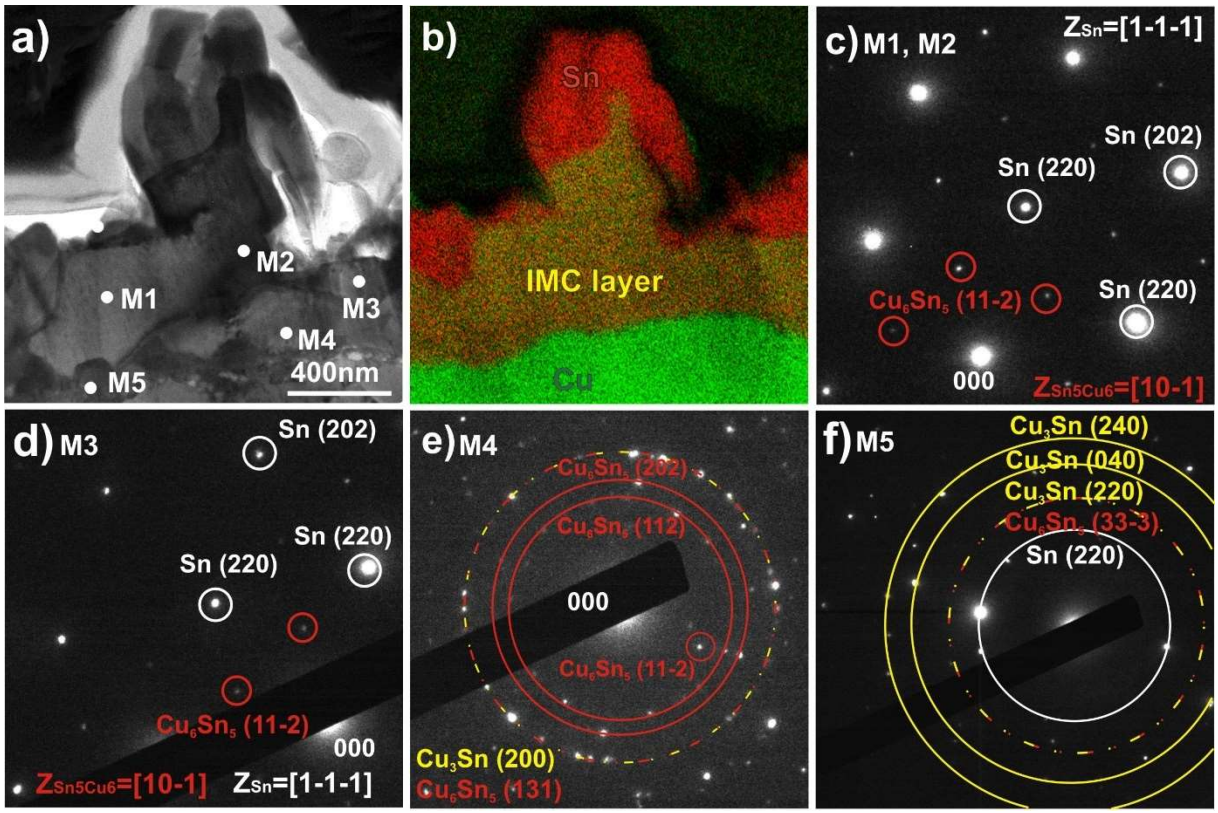

Fig. 4. TEM analysis of a nodule whisker and the area underneath (S2): a) TEM bright field (BF) image; b) EDS element map; c)-f) TEM diffraction patterns at M1-M5 points [8].

Close to the Sn whisker roots, monocrystalline Cu_6Sn_5 grains were found (Fig. 4.c, d), while further from the whisker roots, they are usually polycrystalline (Fig. 4. e, f). This phenomenon might be explained by the high elastic anisotropy of the Cu_6Sn_5. The Young's modulus of the monocrystalline Cu_6Sn_5 with preferred orientation can be much higher than Young's modulus of the polycrystalline Cu_6Sn_5. This means higher compressive stress generated by the monocrystalline IMCs compared to the polycrystalline ones. However, the literature is not straightforward about Young's modulus value of monocrystalline Cu_6Sn_5 [8].

A further direction of Sn whisker studies from thin films was the investigation of whisker growth from 99Sn0.3Ag0.7Cu (SAC0307)+Mn07 and 99Sn0.3Ag0.7Cu (SAC0307)-Bi1-Mn07 solder alloys [9, 10]. Ultra-thin film layers (~100-150nm) were vacuum evaporated from the solder alloy onto Cu substrates. The layers were kept at room temperature for 28 days. In the case of the SAC0307-Mn07, the mechanical stress due to the IMC layer growth resulted in whisker formation right after the layer deposition. Most of the whiskers developed in the first 2 weeks of the study since the IMC grains consumed the ultra-thin film layer. The whisker density was extremely high (~24000 pcs./mm^2). Most of the whiskers were the short nodule

type, which does not mean risk in microelectronics. However, the Mn addition limited the filament whisker development effectively, in the number and in the maximal length, too [9].

Bi addition could increase the stress relaxation ability of the ultra-thin film layer; the whisker formation started only three days after the evaporation in the case of the SAC0307-Bi1-Mn07 layer. The Bi addition could decrease the Bulk modulus of the alloy; this effect and the separately formed Bi grains could increase the relaxing ability of the SAC0307-Bi1-Mn07 layer. Besides, the SAC0307-Bi1-Mn07 alloy could entirely suppress the formation of filament-type whiskers that might cause reliability issues in microelectronics. Furthermore, a unique phenomenon was observed that the SAC0307-Bi1-Mn07 layer produced mostly Bi–Sn whisker couples (Fig. 5). This might be caused by the mechanical stress transfer from the stressed Sn grain to the neighbouring Bi grain, which also reacted to the stress by whisker formation [10].

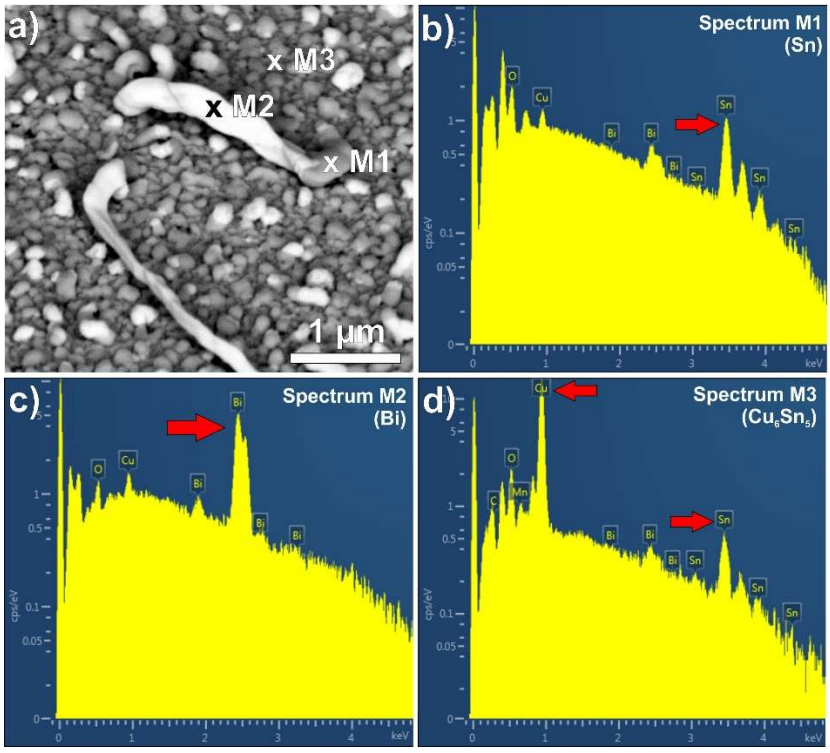

Fig. 5. Whiskers on SAC0307-Bi1-Mn07 thin film layer at 28 days after the evaporation: a) SEM-BSE micrograph; b-d) EDS spectrum of the layer and a whisker [10].

3. Quality and application of composite solder alloys

A preparatory step of the composite solder alloy development was the investigation of wetting properties of different high tin-content solder alloys on Printed Circuit Boards (PCBs) with different thermal capacities [11]. The following solder alloys were used: INNOLOT (SnAg3.8Cu0.7Bi3Sb1.4Ni0.15), SACX Plus 0307 (SnAg0.3Cu0.7Bi0.1Ni0.05), SACX Plus 0807 (SnAg0.8Cu0.7Bi0.1Ni0.05), SACX 0807 (SnAg0.8Cu0.7Bi0.1) and SAC305

(Sn96.5Ag3.0Cu0.5). Glass fiber reinforced FR4 epoxy resin boards were used with a copper foil on one side. The thickness of the boards was: 0.25, 0.5, 1, 1.5 and 2 mm. Spreading tests with 2.3 mm round apertures were used to investigate the wetting properties. The tests were evaluated according to the size of the wetted area and the contact angle of the solder spot. It was found that the thermal capacity (the thickness) of the PCB does not have any considerable effect on the wetting properties. Only minor differences were obtained between the different alloys in the wetted areas. The results were between 19.5 – 21.5 mm^2. However, the wetting angles showed larger differences between 4–7° (the lowest angle is better from the point of wetting). The SAC305 and the SACX plus 0307 solder alloys showed the best performance [11]. So, these solder alloys were selected for further investigation.

The influence of the soldering profile on the thermal parameters of SAC solder joints was also studied [12]. IGBT transistors were soldered with SACX0307 solder paste, applied to different soldering ovens, and at different temperature profiles. It was found that both the soldering technology used and the thermal profile could change the thermal impedance $Z_{th}(t)$ and thermal resistance Rth. The differences were between 15% and 20% for $Z_{th}(t)$ and Rth, respectively (Fig. 6).

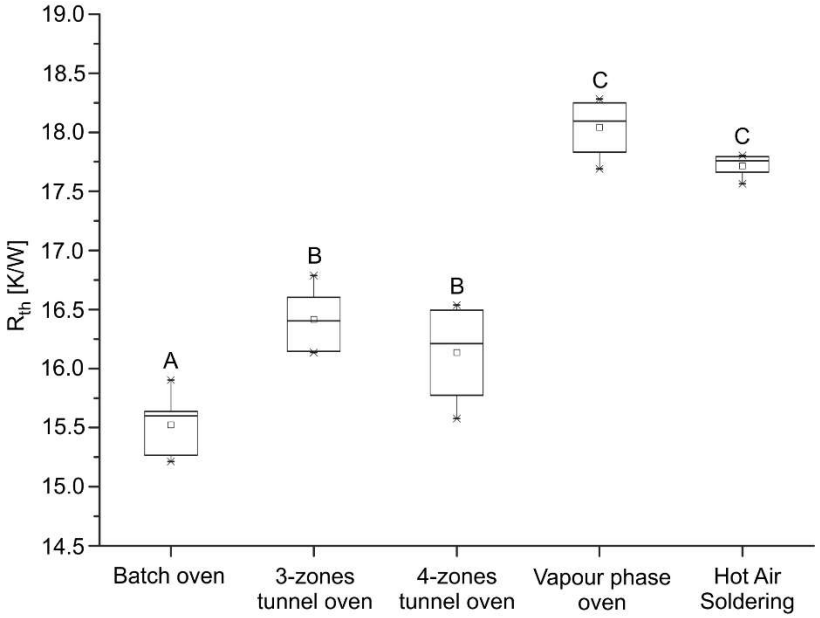

Fig. 6. Thermal resistance (Rth) of NGB8207BN transistors soldered onto FR4 substrate in different soldering ovens [12].

The best results were observed in the case of a batch oven with infrared heating. Although the ratio of the gas void in the solder joints varied between 3% and 30%, no correlation between the void ratios and R_{th} value increase was found. Significant differences were found in the

intermetallic layer thicknesses in the case of the different soldering technologies, which correlated well with the time above liquidus during the soldering process. The thermal parameters of the IGBT assembly could be changed due to the increased thermal conductivity of the IMC layer as compared to that of the bulk solder joint [12].

Furthermore, it was investigated how the flux content of the solder paste affects the intermetallic layer growth [13]. The dependence of intermetallic layer thickness on ROL0 / ROL1 flux classification, glossy or matt solder mask, and OSP / HASL / ENIG soldering pad surface finish was studied. The influence of multiple reflows was also observed. The intermetallic layer thicknesses were obtained by the image analysis of micro-section images. The flux type proved to have a significant impact on the intermetallic layer thickness. The solder paste with ROL1 caused an increase in intermetallic layer thickness by up to 40% in comparison to an identical paste with ROL0 flux. Furthermore, doubling the roughness of the solder mask has increased the resulting intermetallic layer thickness by 37% at HASL surface finish and by an average of 22% [13].

Different etching methods (simple chemical etching, deep etching based on the Jackson method, and selective removal of Sn by a standard three-electrode cell method.) have been applied on SAC305 solder joints [14]. The micrographs prepared by electrochemical etching revealed the best observations regarding the shape and texture of the IMC phases. The reduction in the XRD peak intensities showed the influence of the cooling condition on the formation of the different phases. The Ag_3Sn network was significantly refined, and the thickness of the Cu_6Sn_5 layer decreased with an increase in the cooling rate. It was the result of the reduced solidification time [14].

In the next step, the microstructure of the Mn-doped SAC0307 alloy (0.1, 0.4, 0.7wt%) was investigated in the case of different cooling rates from 0.3 to 4.5 K/s [15]. Even 0.1wt% of Mn can significantly alter the microstructure. Due to the grain refinement effect of the Mn, no β-tin dendrites can be formed, and the Ag_3Sn IMCs are not only present inside the interdendritic regions but they are structurally distributed inside the solder. Independently of the cooling rate of the solder samples, the microstructure of the Mn-containing solder alloys remained stationary. It suggests that the macroscopic properties are also expected to be less sensitive to the cooling rate of the solidification. A significantly higher amount of Mn particles had been observed close to the substrate of the solder, which might be in correlation with the directionality of the solidification of the solder joints since the solder is solidifying from the top to the bottom [15].

Furthermore, the mechanical properties of the Mn-doped SAC0307 and SAC305 were compared in the case of different cooling rates (from 2.7 K/s to 14.7 K/s) [16]. The mechanical properties were not significantly changed over the different cooling rates, but differences in the microstructures were observed. The SAC0307-Mn07 alloy behaved systematically softer against mechanical load than the SAC305 alloy, which makes the SAC0307-Mn07 a promising creep-resistant alloy for long-term operation. The morphology of the IMC layer at the solder–substrate interface was rougher in SAC0307-Mn07 than in SAC305 solder joints (Fig. 7). The rougher the surface of the solder–substrate interface, the more difficult it is for the crack to propagate so that the SAC0307-Mn07 solders could improve their resistance against a cyclic external load (like vibration and cyclic thermal load) [16].

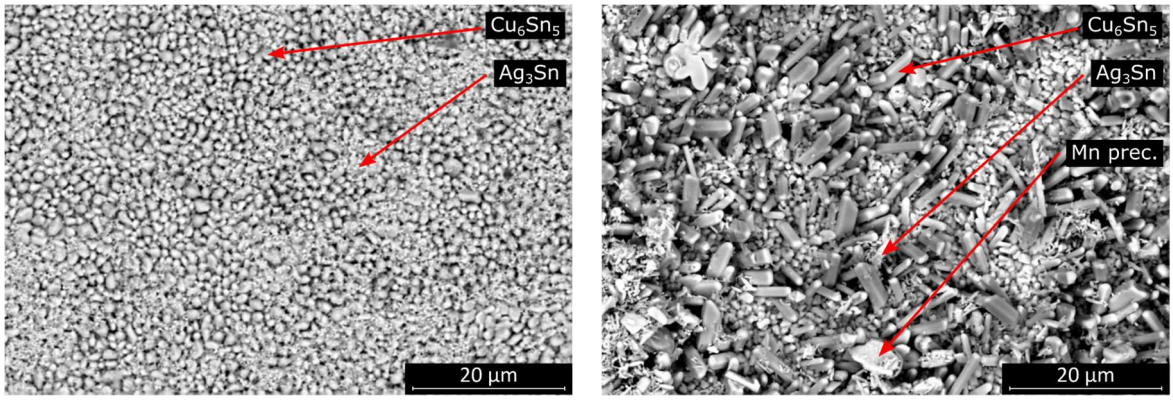

a) b)

Fig. 7. SEM micrographs of the exposed IMC layer of the samples cooled at the rate of 14.7 K/s: a) SAC305; b) SAC0307-Mn07 [16].

The investigation of composite solder alloys was started with SAC305 solder alloy, which was reinforced with 1.0 wt % of TiO_2 nano-particles, using a ball milling process. The aim was to study the changes in the microstructure and the mechanical properties of the composite solder alloy [17]. X-Ray Diffraction (XRD) analysis showed that the TiO_2 nano-particles were successfully blended into the SAC305 solder paste. The slight increase of the TiO_2 peak intensity at the lower cross-sections suggested a favorable distribution of the TiO_2 nano-particles at the particular region. SEM micrographs about the solder/substrate interface showed that the SAC305-1.0T solder composite contains dot-like Ag_3Sn, while the SAC305 contains needlelike Ag_3Sn. In addition, the presence of TiO_2 nano-particles resulted in the size reduction of Cu_6Sn_5 phases.

The improvement in the hardness of the composite solder alloy was analyzed by nanoindentation (Fig. 8). A specific indentation array was performed on four different

horizontal cross-sections of the composite solder with different heights and diameters in order to verify the mixing homogeneity of TiO_2 nano-particles. Incorporation of the 1.0 wt % TiO_2 nano-particles improved the hardness values up to 26.2% than that of pure SAC305 (Fig. 6). The hardness values increased gradually from the top towards the solder/substrate interface. The refined Ag_3Sn and Cu_6Sn_5 IMC phases, due to the presence of the TiO_2 nano-particles, significantly restrained the dislocation movements during mechanical load, which was responsible for improving the hardness of the solder joints [17].

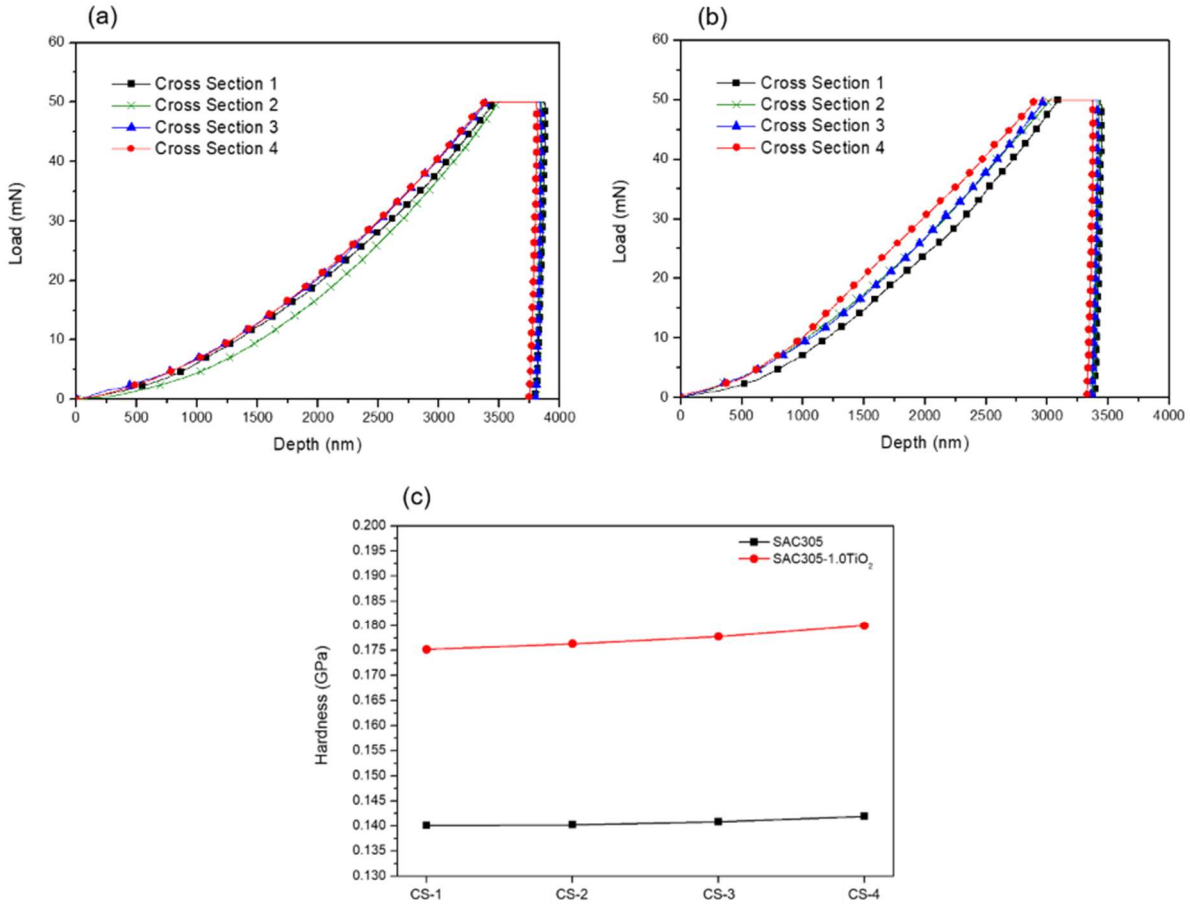

Fig. 8. Load-depth hysteresis comparison of the cross-sections: (a) SAC305 solder alloy; (b) SAC305-1.0TiO2 solder alloy; and (c) the generated hardness profiles of the solder alloys [17].

The microstructural analysis of 95.5Sn-3.0Ag-0.5Cu-1.0TiO_2 composite solder alloy was continued with selective electrochemical etching [18]. Cyclic voltammetry and chronoamperometry were used to investigate the selective etching performances. Successful observation of the TiO_2 near the Cu_6Sn_5 layer was attained for an optimum etching duration of 120s. Clusters of TiO_2 nanoparticles were entrapped by Cu_6Sn_5 IMC layer and by the thread-

like Ag_3Sn IMC particles at the solder/substrate interface. The presence of TiO_2 nanoparticles at the solder interface suppressed the growth of the Cu_6Sn_5 IMC layer and refined the grain morphology of β-Sn. The refined grain morphology helped the β-Sn dissolution, which resulted in a higher amount of removed β-Sn. The absence of a β-Sn matrix also subserved the more depth morphological observations of the Cu_6Sn_5 and Ag_3Sn IMCs as well as the TiO_2 reinforcement particles [18].

The application of ceramic reinforcements in high Sn-content solder alloys was continued with the application of ZnO nano-particles in SAC0307-based composite solder alloys [19]. The primary ZnO particle sizes were 50, 100, and 200 nm. They were added to a solder paste at a ratio of 1.0 wt %. The ZnO nano-particles decreased the wettability, and this increased the voiding of the composite solder joints (Fig. 9).

Fig. 9. Three-dimensional (3D) CT image of a SACX0307-ZnO-(50 nm) solder joint [19].

The wetting decrease corresponded to the primary particle size of the nano-particles (50–200 nm). The ZnO ceramic refined the Sn grains by one order of magnitude, refined the Ag_3Sn IMC particles by ~70%, and decreased the thickness of the IMC layer by ~45%. These microstructural changes could compensate for the negative effect of excessive void formation, as the shear strength and the thermoelectric parameters of the composite solder joints remained almost the same compared to the SACX0307 reference. The refining effects of the ZnO particles strengthened the load-transfer ability of the solder joints, but the decreased IMC thicknesses might equalize the shear strength of the solder joints near the reference level. With an improved wetting (using highly activated fluxes) of the ZnO composite solder alloys, their joints could exceed the quality of the reference SACX0307 [19].

Later, the quality parameters of the SACX0307-TiO2 and SACX0307-ZnO composite solder alloys were compared [20, 21]. The nano-particles were mixed into the solder paste in different volume fractions between 0.25 and 1 wt%, using the ball milling process. Printing, wetting, and mechanical tests were performed. It was found that the ceramic reinforcements did not have a considerable effect on the printing and wetting of the composite solder alloys. However, the shear strength of the nano-composite solder joints increased compared to the reference SACX0307. Generally, the application of TiO_2 nano-particles resulted in a bit better soldering properties than the ZnO nano-particles. No straightforward correlation was found between the volume fraction of the ceramic nano-particles and the soldering properties of the nano-composite solder alloys. Expect in the case of the ZnO nano-particles, when the volume fraction should not exceed 0.5wt% since it can inhibit the proper reflow of the solder paste [20]. Furthermore, a computational fluid dynamics model was established aiming to investigate the stencil printing process [21], which will be useful for further investigation of the solderability of the high Sn content solder alloys.

The effect of the primary particle size of the nano-particles was also investigated [22]. SACX0307-ZnO and SACX0307-TiO2 nano-composite solder pastes were fabricated. The ceramic reinforcements were used in 1wt% and with different primary particle sizes between 50-200nm. The soldering properties of the solder joints were investigated. The nano-particles were mixed into the solder paste by standard ball milling process. Reflow soldering technology has been applied to prepare solder joints and spreading tests from the different solder alloys. The solder joints were evaluated by shear test, and cross-sections were prepared to investigate the metallographic properties by SEM. The wetting property of the nano-composite solder alloys depended on the size and the material of the added ceramics. The TiO_2 nano-particles did not change the wetting properties of the nano-composite solders; however, in the case of the ZnO nano-particles, the wetting behaviour decreased considerably compared to the reference SACX0307. The shear strength of the TiO_2 nano-composite solder joints increased compared to the simple SACX0307. The results of ZnO nano-particles were not obviously positive. ZnO with 200nm primary particles size increased the shear strength; however, in the case of ZnO with smaller primary particle sizes, a considerable shear strength drop was observed. The ceramic reinforcements caused considerable β-Sn grain refinement in each case. In the case of proper wetting, the considerable β-Sn grain refinement could cause the shear strength improvement [22].

In the next step, it was investigated how the previously discussed microstructural changes affect the thermal properties of the composite solder joints [23]. Two different primary particle

sizes were used for reinforcing, which were 20nm (nano) and 200nm (submicron). Power LED modules were fabricated with composite solders. The addition of submicron TiO_2 decreased the thermal and electric thermal resistances of the light sources by 20% and 16%, respectively, and it slightly increased the luminous efficiency (Fig. 10). Microstructural evaluations showed that the precipitated TiO_2 particles at the bottom of the solder joints decreased the thermodynamic energy of Cu_6Sn_5 nucleation since the Cu_6Sn_5 prefers to nucleate on the TiO_2 particles. It refined the Cu_6Sn_5 grains in the composite solder joints and changed the IMC layer structure from elongated scallop-type to rough scallop-type. The adsorption of TiO_2 particles into the Cu_6Sn_5 grains suppressed the growth of Cu_6Sn_5 IMC layer and enhanced the spalling of Cu_6Sn_5 grains to the solder bulk. The modified IMC structure of the composite solder joints decreased their thermal resistance and resulted in better luminescence properties in power LED assemblies [23].

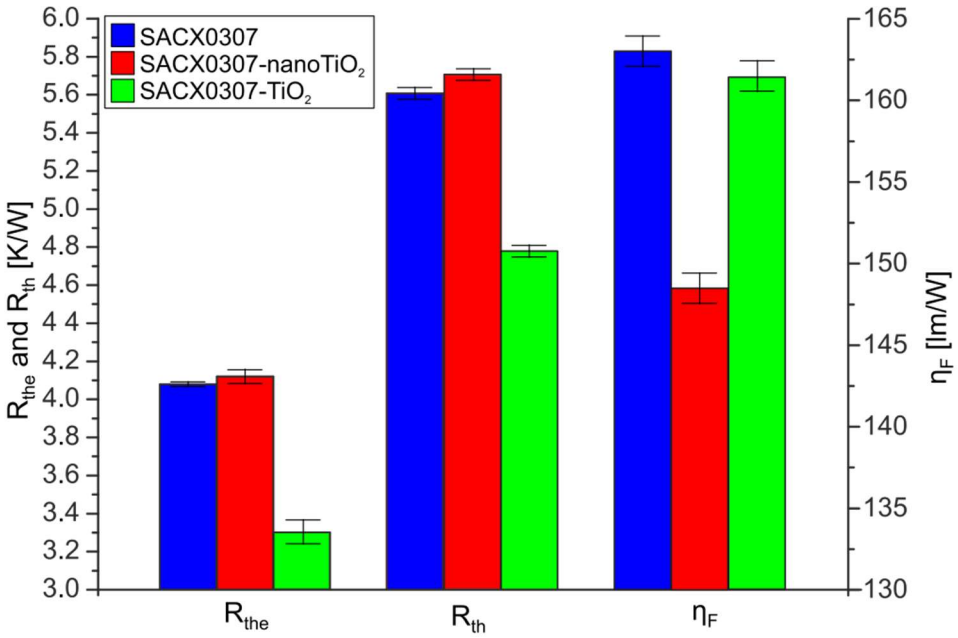

Fig. 10. Thermal resistance (R_{th}), electric thermal resistance (R_{the}), and luminous efficiency η_F) of the tested diodes soldered by different soldering pastes (I_{Fmax} = 5A) [23].

The influence of SAC0307-ZnO composite solder alloy on the optical and thermal parameters of power light-emitting diodes (LEDs) was also investigated [24]. Three different SACX0307-ZnO composite solder alloys were fabricated with different primary particle sizes: 50, 100 and 200 nm. The reference sample was SACX0307. It was proven that ZnO ceramic reinforcement in all solder alloys increased the thermal parameters of LEDs and decreased the η_F luminous efficiency. Thermal resistance R_{th} values were 10% higher and ΔT_j 20% higher for the samples soldered with composite solder alloy than the reference sample. Simultaneously η_F

dropped by 32%. Meanwhile, the optical efficiency η_{OPT} stayed on the same level for all samples. The results showed that ZnO addition to the solder paste at a level of 1wt% did not improve the thermal and optical parameters of LED assemblies. It is assumed that the lowest ZnO content in the solder paste could give better results [24].

At the end of the quality parameters investigations, a new type of nano-particle has also been tested, the SiC. The effect of SiC nano-phases (nano-particles and nano-fibers) addition into SAC0307 solder paste was investigated on the thermal and microstructural properties of the composite solder joints. The nano-phases were used between 0.125 and 1 wt%, and they were mixed into the solder paste by ball milling process. For the study power MOSFET (metal oxide semiconductor field effect transistor) components were soldered onto metal core printed circuit boards (MCPCBs). The thermal impedance Zth(t) and thermal resistance Rth of MOSFETs were measured by an indirect electrical method. Furthermore, the void formation and the microstructure of solder joints were also studied [25].

Despite the nano-phases increased the void formation in the solder joints. Any other amount of SiC nano-phases resulted in slightly worse or similar thermal parameters than the samples soldered with the reference SAC0307 alloy. It was proven that not only from the wettability or the microstructure but from the point of thermal behavior as well, the optimal amount of SiC in the composite solder joints is around 0.5wt%. In the case of the SiC nano-fibers, only a decrease in the IMC layer thicknesses was observed (Fig. 11). The thinner IMC layers could explain the better thermal parameters of the composite solder joints since the SnAgCu solder alloys have better specific thermal conductivity than the Cu_6Sn_5 IMC. Better thermal parameters of the SiC composite solder joints could be achieved by decreasing the voids in them. Generally, the application of SiC nano-particles for soldering power electronics is suggested, but only in around 0.5wt% amount [25].

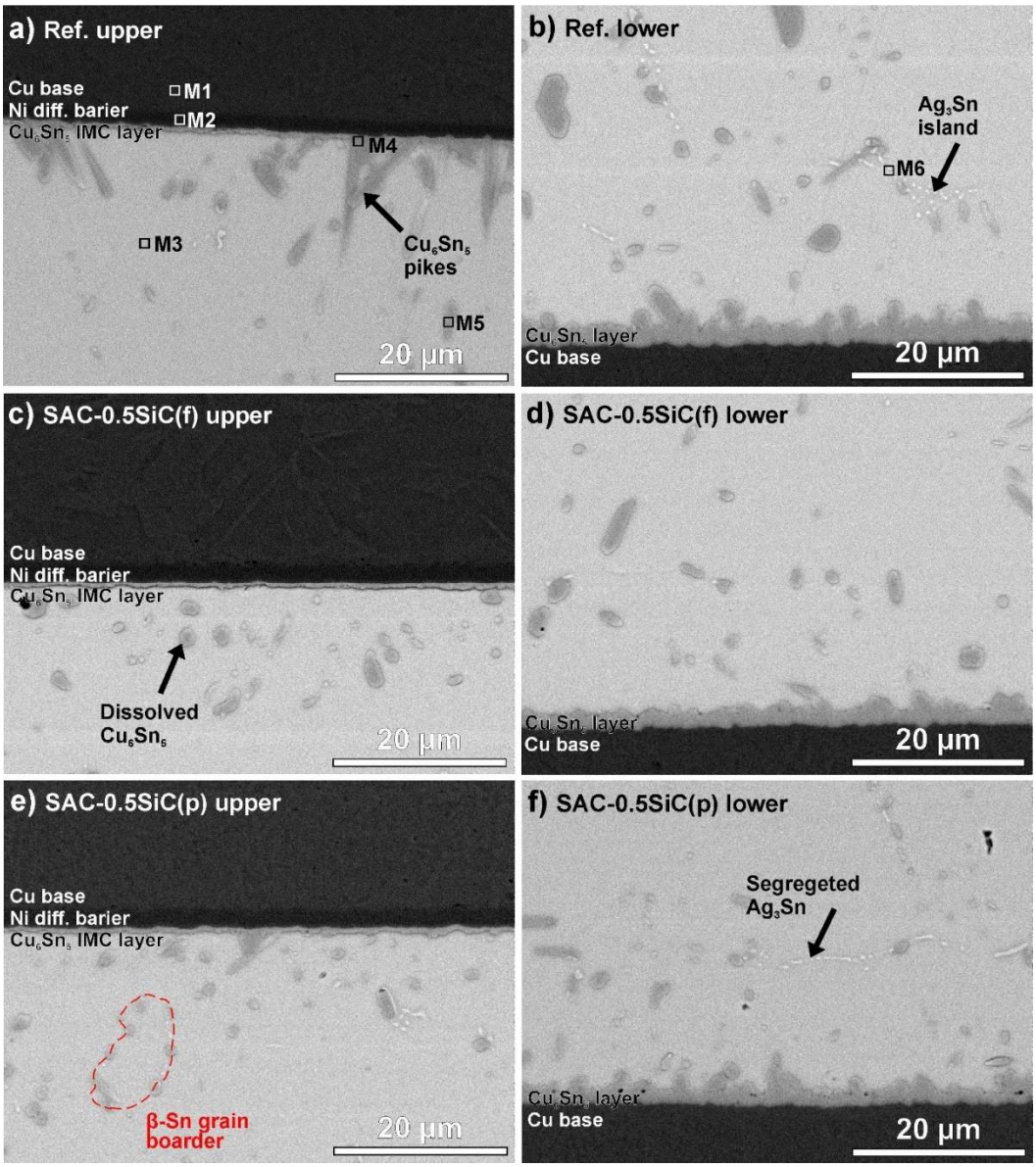

Fig. 11. Structure of the IMC layers in the solder joints: a) Ref. upper IMC layer; b) Ref. lower IMC layer; c) SAC-0.5SiC(f) upper IMC layer; d) SAC-0.5SiC(f) lower IMC layer; e) SAC-0.5SiC(p) upper IMC layer; f) SAC-0.5SiC(p) lower IMC layer [25].

4. Reliability of composite solder alloys

The Sn whisker susceptibility of the above discussed composite solder alloys was studied. Sn whisker growth has been observed from SAC0307-ZnO [26] and SAC0307-TiO_2 [27] composite solder joints. The commercial SAC0307 solder alloy was reinforced by ZnO and TiO_2 nano-particles, which resulted in composite solder joints. The nano-particles were mixed into the solder paste in a 0.25 wt% volume fraction, using the ball milling process. Solder joints were prepared from the composite solder alloy and from the reference SAC0307, on Ag surface

finish by conventional SMT. The solder joints were exposed to an accelerated lifetime test (85 ºC/85 RH% THB, 4000 hours) to enhance the Sn whisker growth.

Corrosion spots were observed after 1000 hours of aging, and the first whiskers appeared after 1500 hours of aging on the reference SAC0307 solder joints. In the case of the ZnO and TiO_2 composite solder joints, none of the previous phenomena were observed during 4000 hours of THB aging. The microstructural analysis of the reference SnAgCu solder alloy showed that the volumetric increase of the corroded β-Sn grains resulted in local mechanical stress in the solder joints, which was released by Sn whisker development (Fig. 12).

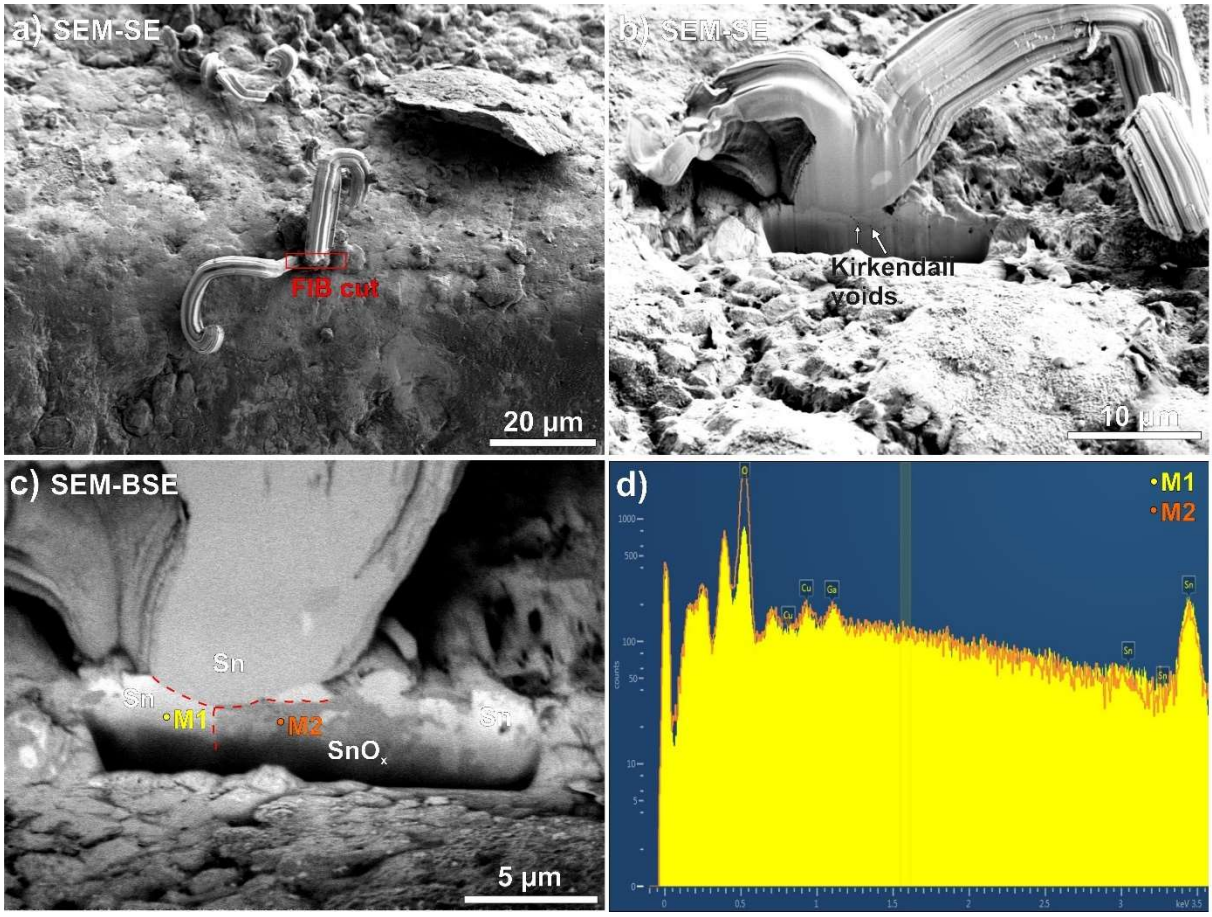

Fig. 12. Sn whisker couple on the SAC0307 solder joint: a) nodule Sn whiskers; b) SEM-SE micrograph of the FIB cut at the root of the whiskers; c) SEM-BSE micrograph of the FIB cut at the root of the whiskers; d) EDS result of the Sn grains at the root of the whisker [27].

However, in the composite solder joints, the increased grain boundary fraction and segregation of the TiO_2 and ZnO nano-particles to the grain boundaries resulted in a relatively uniform and compact protective oxide layer at the β-Sn grain boundaries (Fig. 13). This suppressed the formation of SnOx, and via this, the corrosion-induced whisker growth. Therefore the

application of reinforcement TiO_2 and ZnO nano-particles is favorable for increasing the reliability of SnAgCu solder joints in corrosive environments [26, 27].

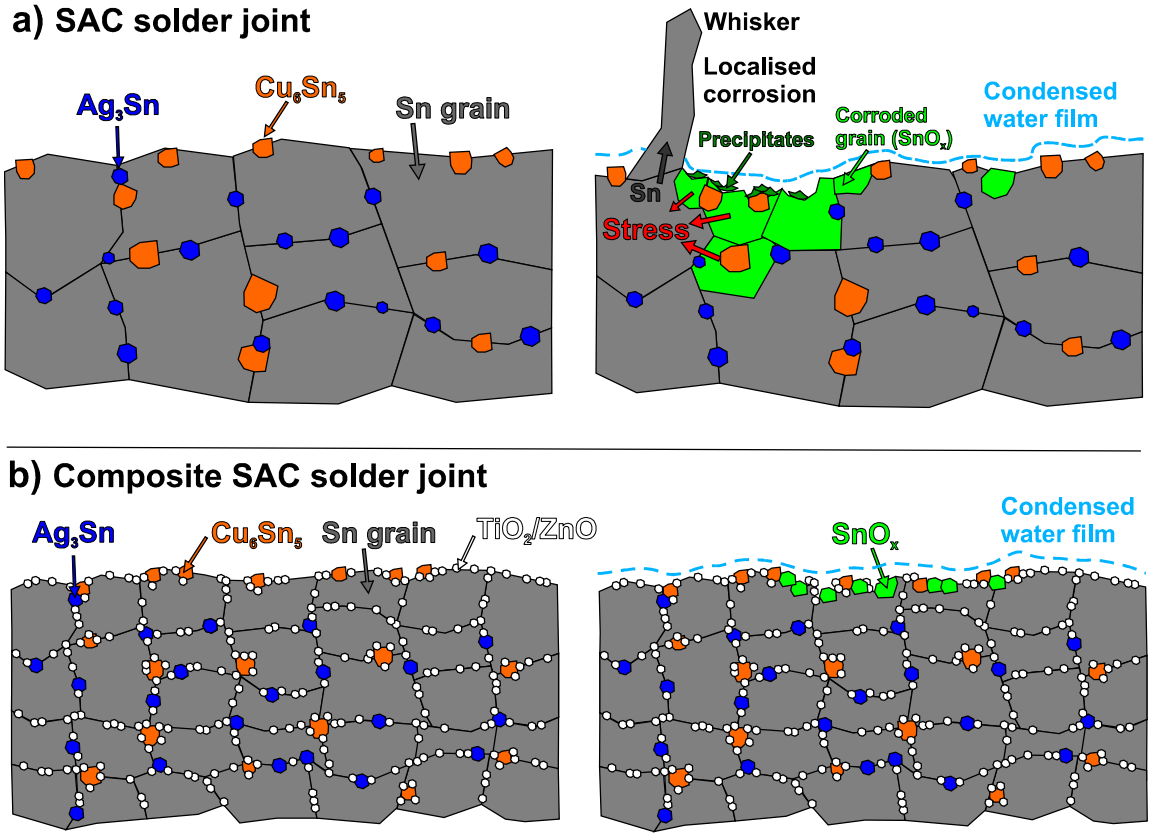

Fig. 13. Schematic illustration of corrosion process on the surface of the solder joints: a) localized corrosion SAC solder joint; b) effect of the protective oxide layer in the case of composite SAC solder joint [27].

The incorporation mechanism of TiO_2 nano-particles into SnAgCu solders [28]. Composite solder alloys have been made from 99Sn0.3Ag0.7Cu solder alloy and TiO_2 nano-particles between 0.25-1 wt%. The alloys in solder joints were exposed to 4000 hours long 85°C/85RH% thermal-humidity test, and their surface was observed by SEM and FIB techniques. Large localized corrosion spots and numerous Sn whiskers have been found on the samples, except for the samples with 0.25wt% TiO_2 content. The non-soluble TiO_2 NPs refined the Sn-matrix and segregated to the grain boundaries. However, differences were found in their distribution in the function of the weight fraction. TiO_2 NPs were incorporated layer-like in the case of lower weight fraction (0.25 wt%). While in the case of higher TiO_2 weight fractions, TiO_2 agglomerates were formed. DFT calculations proved that in soldering conditions, the Sn atoms of the solder alloy could bond to the TiO_2 NPs through the O atoms of TiO_2. The bonded TiO_2-Sn structure is not able to oxidize further (Fig. 14).

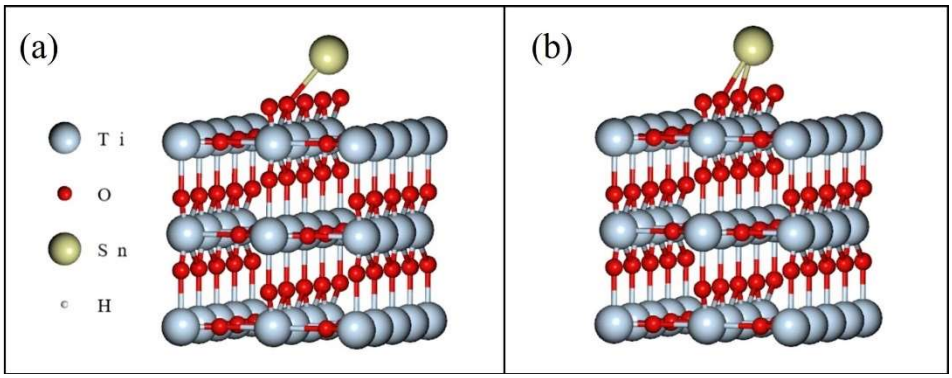

Fig. 14. DFT calculations: a) initial position of the Sn atom on TiO_2 surface; b) calculation results of the Sn atom on TiO_2 surface [28].

So the layer-like incorporation of the TiO_2 NPs (at 0.25wt%) could slow down corrosion and suppress Sn whisker growth. The TiO_2 agglomerates (at 0.5 and 1 wt%) could not perform corrosion protection and whisker mitigation effects. Therefore, applying TiO_2 reinforcing NPs is suggested only in lower weight fractions (below 0.5wt%) to improve the reliability parameters of SnAgCu solder alloys.

In the next step, the reliability of the same SiC composite solder alloys was studied [29]. The solder joints were exposed to accelerated lifetime tests (85°C / 85RH% THB, 4000h). The samples were observed by SEM every 1000 hours of the test. On the SAC0307-SiC composite solder joints, Sn whiskers and large corrosion spots were observed after 1000 hours of the THB test. In the case of SAC0307 reference samples, only minor corrosion signs were found till 3000h of the THB test. The addition of SiC nano-phases promoted Sn whisker growth and decreased the corrosion resistance of the composite solder joints.

The microstructural analysis proved that close to the root of the whiskers, the solder layer suffered serious localized corrosion, and at the upper meniscus Ni_xSn_y IMC layer growth occurred as well. Both phenomena caused volumetric changes in the solder layer, which resulted in mechanical stress at the surface region of the solder joints. The mechanical stress was released by whisker growth. Although the SiC nano-phases can bond to the Sn atoms, but they are prone to corrosion. This results in SiC nano-phases acting as corrosion incubation points in the Sn-matrix, which causes a decrease in the corrosion resistance of the SiC composite solder joints (Fig. 15).

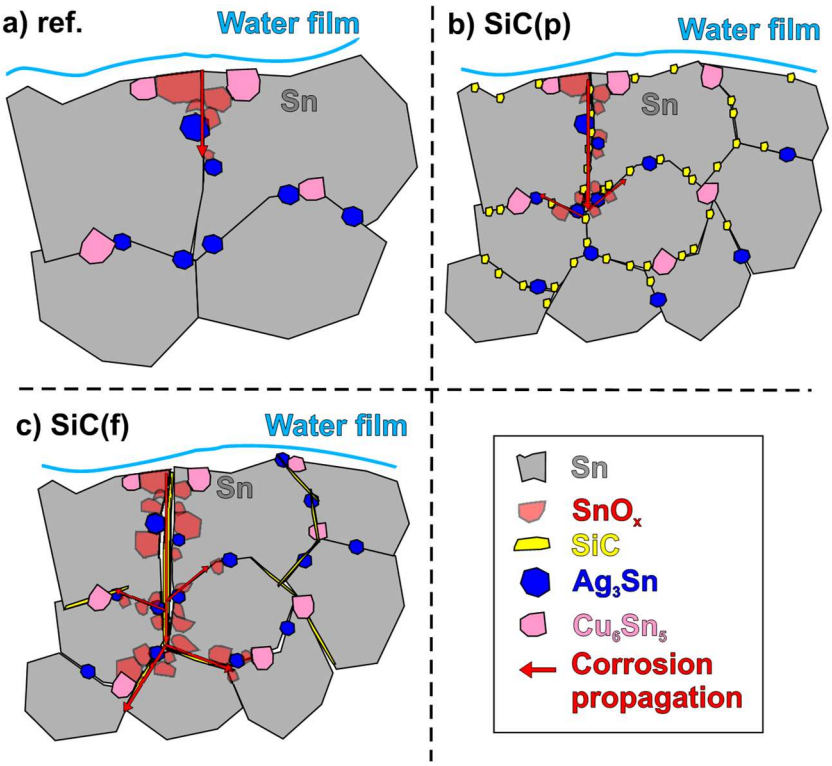

Fig. 15. Corrosion propagation in the solder joints: a) ref.; b) SiC(p); c) SiC(f) [30].

SiC fibers can wedge in deeply between Sn grains and ensure an even faster corrosion propagation towards the solder bulk than SiC powder (Fig. 15). On the upper meniscus, where the Sn layer was thin, the great mechanical stress could grow nodule-type whiskers over 100 μm in length, which is unique but also means a high-reliability risk for the fine-pitch microelectronics components. Therefore, despite the promising solderability and mechanical parameters, using SiC nano-phases in composite soldering is questionable from the reliability aspects [30].

5. Summary

Our research project has investigated the reliability of high Sn-content solder alloys. The duration of the research project was extended from 4 to 5 years due to the COVID-19 situation, which was unfortunate at that time, but finally, it gave us the opportunity to reach even more and even deeper results.

Basically, we aimed two main specific research branches: the tin whisker growth and the tin pest phenomenon from high Sn-content solder alloys. During the 5 year duration of the project, these two main branches have been extended with the investigation of composite solder alloys as well. Accordingly, the focus points of the project have been shifted marginally, but we felt that we cannot omit the progressive improvement of composite soldering. We have reached

considerable scientific findings in the area, and from these, we would like to highlight only the most important ones:

- Showing the positive effect of recrystallization to delay tin pest phenomenon in high Sn content solder alloys.
- Showing and explaining high-risk of Sn whisker growth in the case of sub-micron thick Sn thin films.
- Characterizing the microstructural and thermal parameters of composite solder joints.
- Discovering and explaining the corrosion protection of TiO_2 and ZnO nano-particles in composite solder joints against corrosion and Sn whisker growth.
- Discovering and explaining the high-reliability risk of application of the SiC in SAC solder alloys.
- Characterizing the incorporation of TiO_2 and SiC nano-particles into the solder matrix.

According to our application trials, we see great potential to apply composite solder alloys in power electronics. They proved that with proper manufacturing technology, they can improve the thermal parameters of the power circuit, which is essential nowadays when power electronics are developing fast. Therefore, we are planning to continue our research towards composite soldering.

6. International cooperation

The research project was executed with a wide international cooperation with the following institutes and universities:

- Łukasiewicz Research Network, Institute of Microelectronics and Photonics (former Institute of Electron Technology), Poland;
- Gdynia Maritime Unversity, Poland;
- Czech Technical University in Prague, Czech Republic;
- Dankook University, Department of Physics, Cheonan, Republic of Korea
- Technical University in Košice, Slovakia;
- Universiti Sains Malaysia, Malaysia
- Universiti Malaysia Perlis, Malaysia
- Chulalongkorn University, Thailand

7. Publications:

During the 5 years of the project, we published 30 publications, containing 11 conference papers and 19 journal papers with a sum impact factor of 72.565 (JCR 2022). Furthermore, the principal investigator gave 2 invited talks on international conferences.

[1] B. Illés, A. Skwarek, R. Bátorfi, T. Hurtony, G. Harsányi, Electrical Characterization of β→α-Sn Transition in High Tin Content Solder Alloys with Different Inoculators, ACTA PHYSICA POLONICA A 135/5 (2019) 935-937.

[2] B. Illés, A. Skwarek, T. Hurtony, O. Krammer, G. Harsányi, K. Witek, Characterization of Tin Pest Phenomenon in a Low Ag Content SAC Solder, Proceedings of 22nd EMPC conference 2019:1-5, DOI: 10.23919/EMPC44848.2019.8951853

[3] B. Illés, A. Skwarek, T. Hurtony, P. Zachariasz, G. Harsányi, Investigation of allotropic ß→α-Sn transition in high tin content solder alloys with different microscopy and spectroscopy techniques, ACTA MATERIALIA TURCICA 4 (2020) 20-28.

[4] A. Skwarek, B. Illés, T. Hurtony, K. Dušek, D. Bušek, Effect of recrystallization on ß to α-Sn allotropic transition in Sn99.3Cu0.7 wt% solder alloy inoculated with InSb, MATERIALS 13 (2020) 968.

[5] B. Illés, T. Hurtony, O. Krammer, R. Bátorfi, B. Medgyes, G. Harsányi, Early Stage Whisker Development from Sn Thin Film on Cu Substrate, Proceedings of 42nd IEEE-ISSE conference 2019:1-5., DOI: 10.1109/ISSE.2019.8810272

[6] B. Illés, T. Hurtony, O. Krammer, B. Medgyes, K. Dusek, D. Busek, Effect of Cu substrate roughness and Sn layer thickness on whisker development from Sn thin-films, MATERIALS 12 (2019) 3609.

[7] B. Illés, O. Krammer, T. Hurtony, K. Dusek, D. Busek, A. Skwarek, Kinetics of Sn whisker growth from Sn thin-films on Cu substrate, JOURNAL OF MATERIALS SCIENCE: MATERIALS IN ELECTRONICS 31 (2020) 16314-16323. (IF=2.478)

[8] B. Illés, A. Skwarek, J. Ratajczak, K. Dušek, D. Bušek, The influence of the crystallographic structure of the intermetallic grains on tin whisker growth, JOURNAL OF ALLOYS AND COMPOUNDS 785 (2019) 774-780

[9] B. Illés, R. Bátorfi, T. Hurtony, O. Krammer, G. Harsányi, A. Pietrikova, A. Skwarek, K. Witek, Whisker Development from SAC0307-Mn07 Solder Alloy, Proceedings of 43nd IEEE-ISSE conference 2020:1-5. DOI: 10.1109/ISSE49702.2020.9120879

[10] B. Illés, B. Medgyes, T. Hurtony, O. Krammer, K. Dusek, D. Busek, Sn and Bi Whisker growth from SAC0307-Mn07 and SAC0307-Bi1-Mn07 Ultra-thin film layers, VACUUM 187 (2021) 110121. (IF=3.627 (2020))

[11] M.A. Alaya, L. Gál, T. Hurtony, B. Medgyes, D. Straubinger, A.M. Tareq, B. Illés, A. Géczy, Wetting of different lead free solder alloys during vapour phase soldering, Proceedings of 42nd IEEE-ISSE conference 2019:1-6. DOI: 10.1109/ISSE.2019.8810204

[12] A. Pietruszka, P. Górecki, S. Wroński, B. Illés, A. Skwarek, The influence of soldering profile on the thermal parameters of insulated gate bipolar transistors (IGBTs), APPLIED SCIENCES 11 (2021) 5583.

[13] K. Dušek, P. Veselý, D. Bušek, A. Petráč, A. Géczy, B. Illés, O. Krammer, Influence of Flux and Related Factors on Intermetallic Layer Growth within SAC305 Solder Joints, MATERIALS 14 (2021) 7909.

[14] M.Z. Yahaya, N.A. Salleh, S. Kheawhom, B. Illés, M.F.M. Nazeri, A.A. Mohamad, Selective Etching and Hardness Properties of Quenched SAC305 Solder Joint, SOLDERING & SURFACE MOUNT TECHNOLOGY 32/4 (2020) 225-233.

[15] T. Hurtony, O. Krammer, B. Illés, P. Gordon, Investigation of the Microstructure of Mn-doped Tin-Silver-Copper Solder Alloys Solidified with Different Cooling Rates, Proceedings of 22nd EMPC conference 2019:1-5, DOI: 10.23919/EMPC44848.2019.8951866

[16] T. Hurtony, O. Krammer, B. Illés, G. Harsányi, D. Busek, K. Dusek, Investigation of the mechanical properties of Mn-alloyed tin-silver-copper solder solidified with different cooling rates, MATERIALS 13 (2020) 5251.

[17] S.S.M. Nasir, M.Z. Yahaya, A.M. Erer, B. Illés, A.A. Mohamad, Effect of TiO2 Nanoparticles on the Horizontal Hardness Properties of Sn-3.0Ag-0.5Cu-1.0TiO2 Composite Solder, CERAMICS INTERNATIONAL 49 (2019) 18563–18571.

[18] M.Z. Yahaya, M.F.M. Nazeri, S. Kheawhom, B. Illés, A. Skwarek, A.A. Mohamad, Microstructural Analysis of Sn-3.0Ag-0.5Cu-TiO2 Composite Solder Alloy after Selective Electrochemical Etching, MATERIALS RESEARCH EXPRESS 7 (2020) 016583.

[19] A. Skwarek, O. Krammer, T. Hurtony, P. Ptak, K. Górecki, S. Wroński, D. Straubinger, K. Witek, B. Illés, Application of ZnO nano-particles in Sn99Ag0.3Cu0.7 based composite solder alloys, NANOMATERIALS 11 (2021) 1545. (5.076 (2020))

[20] B. Illés, A. Skwarek, O. Krammer, D. Straubinger, B. Lakó, G. Harsányi, K. Witek, Soldering with SACX0307-(TiO2/ZnO) nano-composite solder alloys, Proceedings of 43nd IEEE-ISSE conference 2021:1-6; DOI: 10.1109/ISSE51996.2021.9467652

[21] T.I. Al-Ma'aiteh, O. Krammer, B. Illés, Transient Numerical Modelling of the Pin-in-Paste Technology, APPLIED SCIENCES 11 (2021) 4670.
[22] B. Illés, A. Skwarek, O. Krammer, T. Hurtony, D. Straubinger, J. Ratajczak, G. Harsányi, K. Witek, Properties of nano-composite SACX0307-(ZnO, TiO2) , Proceedings of 23rd EMPC conference 2021:1-6, DOI:10.23919/EMPC53418.2021.9585015
[23] A. Skwarek, P. Ptak, K. Górecki, T. Hurtony, B. Illés, Microstructure Influence of SACX0307-TiO2 Composite Solder Joints on Thermal Properties o Power LED Assemblies, MATERIALS 13 (2020) 1563.
[24] A. Skwarek, P. Ptak, K. Górecki, K. Witek, B. Illés, The influence of SACX0307-ZnO nanocomposite solder alloys on the optical and thermal properties of power LEDs, SOLDERING & SURFACE MOUNT TECHNOLOGY 34/4 (2022) 222-229. (IF = 1.494)
[25] A. Skwarek, B. Illés, P. Górecki, A. Pietruszka, J. Tarasiuk, T. Hurtony, Influence of SiC reinforcement on microstructural and thermal properties of SAC0307 solder joints, JOURNAL OF MATERIALS RESEARCH AND TECHNOLOGY 22 (2023) 403-412.
[26] H. Choi, B. Illés, A. Skwarek, T. Hurtony, Tin Whisker Susceptibility of SAC0307-ZnO Composite Solder Joints, Proceedings of 45th IEEE-ISSE conference 2022:1-5, DOI:10.1109/ISSE54558.2022.9812782
[27] B. Illés, H. Choi, T. Hurtony, A. Skwarek, K. Dusek, D. Busek, Suppression of Sn whisker growth from SnAgCu solder alloy with TiO2 and ZnO reinforcement nano-particles by increasing the corrosion resistance of the composite alloy, JOURNAL OF MATERIALS RESEARCH AND TECHNOLOGY 20 (2022) 4231-4240.
[28] B. Illés, H. Choi, J. Byun, K. Dusek, D. Busek, A. Skwarek, Incorporation and corrosion protection mechanism of TiO2 nano-particles in SnAgCu composite alloys: experimental and density functional theory study, CERAMICS INTERNATIONAL 49 (2023) 23765-23774.
[29] H. Choi, A. Skwarek, T. Hurtony, J. Byun, B. Illés, Study of whisker growth from SAC0307-SiC composite solder alloy, Proceedings of 46th IEEE-ISSE conference 2022:1-4, DOI: 10.1109/ISSE57496.2023.10168371
[30] H. Choi, B. Illés, T. Hurtony, J. Byun, A. Géczy, A. Skwarek, Reliability problems of SnAgCu-SiC composite solder joints in corrosive climate, CORROSION SCIENCE 224 (2023) 111488.